Self-diffusion and defect annihilation in nanocrystalline Fe films probed by neutron reflectometry

Sujoy Chakravarty and Harald Schmidt*
Institute of Metallurgy, Materials Physics Group, Clausthal University of Technology, Robert-Koch-Str. 42, D-38678 Clausthal-Zellerfeld, Germany

Ursula Tietze and Dieter Lott
GKSS Research Center Geesthacht GmbH, Max Planck Str. 1, D-21502 Geesthacht, Germany

N. P. Lalla and Ajay Gupta
UGC–DAE Consortium for Scientific Research, Khandwa Road, Indore 452017, India
(Received 16 April 2009; revised manuscript received 30 June 2009; published 22 July 2009)

Self-diffusion in ion-beam-sputtered nanocrystalline Fe is studied between 310 and 510 °C, using neutron reflectometry on $[^{nat}Fe(7\ nm)/^{57}Fe(3\ nm)]_{15}$ isotope multilayers. Neutron reflectometry has the advantage over other methods of diffusivity determination, that diffusion lengths on the order of 1 nm and below can be determined. This enables diffusion experiments in a nanostructure which is not significantly modified by grain growth during annealing. The determined diffusivities are time depended and decrease by more than two orders of magnitude during isothermal annealing. In early stages, diffusion is controlled by frozen-in nonequilibrium point defects (interstitials or vacancies) present after deposition. The decrease in the diffusivities can be attributed to the annihilation of these point defects. For very long annealing times the diffusivities above 400 °C are in good agreement with volume diffusivities measured in single crystals given in literature. However, at a temperature of 400 °C and below the diffusivities are still higher than extrapolated literature data also after more than 8 days of annealing, indicating that defect annihilation is still going on.

DOI: 10.1103/PhysRevB.80.014111 PACS number(s): 66.30.Fq, 66.30.Pa, 61.05.fj

I. INTRODUCTION

Nanocrystalline metals show in comparison to their coarse-grained counterparts, a series of improved mechanical properties for technical applications. These are high hardness, high fracture toughness, and high wear resistance.[1–5] The reason for these enhanced properties is the low grain size on the order of 10–100 nm. A significant fraction of grain-boundary regions is present which separates the crystallites. For example, a nanocrystalline metal with a grain diameter of l_d=20 nm contains 5–15 % grain-boundary phase. The small size of the crystallites limits the conventional movement and multiplication of dislocations and according to the Hall-Petch relation, $\sigma=\sigma_0+k/l_d^{1/2}$, an enhancement of flow stress σ and consequently of hardness occurs (k and σ_0 are constants).[2]

In nanocrystalline metals diffusion of the constituting atoms plays a central role for materials properties and thermal stability, especially at low temperatures close to room temperature. Grain boundaries may serve as a transport path for atoms to a large extent. Due to the reduced dislocation activity in nanocrystalline materials, self-diffusion may gain on importance for plastic deformation, where grain-boundary creep and grain-boundary sliding may become dominant.[5] Self-diffusion also controls the stability of the nanostructure in metals. At relatively low temperatures diffusion-controlled grain growth[6] and also structural relaxation of the grain boundaries takes place.[7] This in reverse may again influence mechanical, electrical, and also magnetic properties. As recently shown in a series of publications,[8,9] in nanocrystalline Fe with average grain diameters below 150 nm abnormal grain growth with linear growth characteristics occurs, which is directly influenced by volume diffusion. During grain growth, excess-free volume located in the grain boundaries is transferred to the volume in form of vacancies. Further, the movement and annihilation of vacancies (which control self-diffusion in metals) may have a strong influence on the creation and relaxation of residual stresses in metals.[10] In conclusion, it can be stated that the mechanisms of mechanical deformation, grain growth, stress modification, and defect annihilation at low temperatures can only be explained and modeled by a fundamental understanding of self-diffusion.

Self-diffusion in nanocrystalline metallic alloys and also impurity diffusion in pure nanocrystalline metals were and are under lively investigation (for an overview see Ref. 7). However, self-diffusion experiments in pure nanocrystalline metals are very limited.[7] This is mainly caused by the fact that during diffusion experiments carried out by classical methods, such as radioactive or stable tracers methods in combination with sputter sectioning, often diffusion-controlled grain growth simultaneously takes place to the actual diffusion experiment (see, e.g., Ref. 11). Consequently, the actual nanostructure is modified during the diffusion experiment and the obtained results are of limited significance. In a simple picture, growth of nanosized grains occurs due to the jump of atoms across the grain boundary with dimensions of 0.5–2 nm and diffusion along the grain boundary. During a diffusion experiment the average displacement of atoms is given by the diffusion length, which defined in one dimension as $d=(2Dt)^{1/2}$ (t: annealing time and D: diffusivity). The minimum diffusion length which can be determined by classical methods is limited to 10–20 nm. This means that over these dimensions during diffusion experiments grain growth may take place. Grains with a typical diameter of about 30 nm may double their size during a diffusion experiment, as observed in Ref. 11. A possibility to

 ©2009 The American Physical Society

overcome this problem is to determine diffusion lengths which are drastically smaller than the actual grain size, best on the order of 1 nm and below. Thus, no significant modification of the actual nanostructure is expected during the diffusion experiment. Such experiments can be realized by a method which is based on isotope multilayers and neutron reflectometry, as recently demonstrated for amorphous[12] and single crystalline systems.[13] In the present study it will be shown that this method can also be applied for the study of self-diffusion in nanocrystalline metals. For our experiments we chose bcc α-Fe as a typical nanocrystalline model system.

II. EXPERIMENT

For the neutron reflectometry experiments, isotope multilayers are necessary. These are thin films which are produced by the alternate deposition of nanometer-sized layers made of different stable isotopes of an element.[14] In the present case $[^{nat}Fe(7\ nm)/^{57}Fe(3\ nm)]_{15}$ structures were deposited by ion-beam sputtering on a Si substrate at room temperature in Argon using natural Fe and ^{57}Fe enriched targets. A voltage of 1000 V and a current of 20 mA at a base pressure of 1×10^{-7} mbar was used. After deposition chemically homogeneous films with a thickness of 150 nm are obtained, which are isotope modulated in the direction perpendicular to the surface. Due to the large difference in neutron-scattering lengths of ^{57}Fe (2.3 fm) and ^{nat}Fe (9.45 fm) this system is well suited for our studies.

Neutron reflectometry experiments were carried out using the polarized neutron reflectometer PNR at the Geesthacht Neutron Facility (GeNF), located at the GKSS research center (Germany). The neutron flux at the sample position in case of polarized neutrons is 3×10^4 neutrons/(cm^2 s). The reflectometer was operated in angle-dispersive ($\theta/2\theta$) mode using a monochromatic neutron beam at a wavelength of 0.635 nm with a wavelength resolution of 5%. Due to the fact that the Fe films are ferromagnetic and neutrons with different spin orientation are reflected differently we used only polarized neutrons with its spin-up component (R+) for the experiments. This helps to increase the sensitivity of the method for diffusivity determination. During reflectivity measurement a vertical field of 30 mT was applied on the sample using an electromagnet. A two-dimensional position-sensitive ^{3}He counter is used for detecting the reflected neutrons.

Isothermal diffusion annealing was carried out in the range between 310 and 510 °C in a vacuum better than 2×10^{-7} mbar using a self-made resistance furnace. TEM studies were done using a Tecnai-G2–20 machine with *W* filament operating at 200 kV. The cross-sectional specimens for TEM study were prepared following standard techniques. Final thinning of the sample was made by Ar ion-beam polishing.

III. RESULTS AND DISCUSSION

Figure 1 shows cross-sectional transmission electron microscopy micrographs of (a) an as-deposited Fe isotope multilayer sample and (b) for a sample annealed at 400 °C for 231 h. From these images we see that the as-deposited sample is composed of columnar grains oriented perpendicular to the film surface. The columnar grains have diameters of about 10–20 nm and a length, which is approximately the film thickness. For the sample annealed at 400 °C, the microstructure and grain size is not significantly modified. As obvious from nearly continuous diffraction rings in the selected area electron-diffraction patterns (not shown), no significant texture is present in the film. The columnar grains grow statistically averaged along different orientations and their growth direction and azimuthal rotations are random. This result is also supported by grazing incidence x-ray diffractometry.

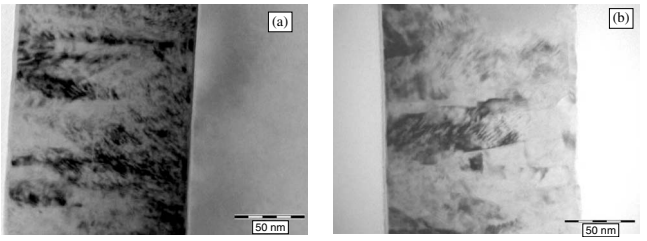

FIG. 1. Cross-sectional bright field-transmission electron images of (a) an as-deposited $[^{nat}Fe(7\ nm)/^{57}Fe(3\ nm)]_{15}$ sample and (b) a sample annealed at 400 °C for 231 h.

A typical neutron reflectometry pattern is given in Fig. 2. A clear Bragg peak is visible at $q_z \approx 0.065$ Å^{-1}, resulting from the reflection of the neutrons at the isotope interfaces and the corresponding interference effects. Isothermal annealing of the isotope multilayers at elevated temperatures leads to interdiffusion of the two isotopes. This results in a decrease in the Bragg peak during isothermal annealing, as shown in Fig. 3 for anneals at 360 °C as a typical example. As obvious from Fig. 3 the Bragg peak decreases to about 25% of its initial value during annealing up to about 213 h. This large reduction demonstrates that the decrease is mainly due to volume diffusion and not due to pure grain-boundary diffusion. In the second case a maximum reduction to about 80–90 % of the initial value only can be expected, corresponding to the amount of grain-boundary phase present in

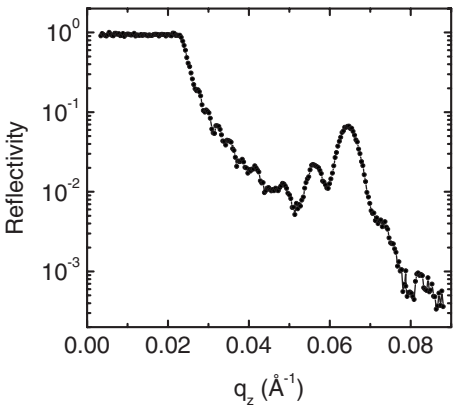

FIG. 2. Neutron reflectivity pattern of an as-deposited nanocrystalline $[^{nat}Fe(7\ nm)/^{57}Fe(3\ nm)]_{15}$ isotope multiplayer probed with polarized neutrons (R^+) at a field of 30 mT.

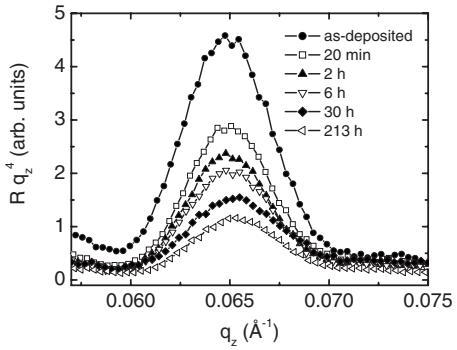

FIG. 3. Decrease in the first-order Bragg peak of a $[^{nat}Fe(7\ nm)/^{57}Fe(3\ nm)]_{15}$ isotope multilayer as a function of annealing time for anneals at 360 °C.

the sample. We assume that diffusion of type B kinetics of Harrison's classification[15] is present, where volume and grain boundaries serve simultaneously as a transport path, while volume diffusion is slower than grain-boundary diffusion. However, volume diffusion dominates the modifications in the reflectivity pattern during annealing in the temperature range investigated.

The self-diffusivities can be calculated according to the expression[14]

$$I(t) = I_0 \exp\left(-\frac{8\pi^2 D}{l^2} t\right), \tag{1}$$

where $I(t)$ is the intensity of the first-order Bragg peak after annealing for time t and l is the bilayer thickness. I_0 is the intensity of the Bragg peak in the as-deposited sample. Diffusivities as a function of annealing time are exemplarily given in Fig. 4(a) for the measurements at 360 °C. Obviously, diffusivity depends drastically on time. It decreases by more than two orders of magnitude with increasing annealing time. The diffusion lengths connected with these diffusivities shown in Fig. 4(b) range of 1.1–1.8 nm. The smallest value measured in this study was 0.8 nm. Such small diffusion lengths cannot be detected by classical methods of diffusivity determination (e.g., the radiotracer technique) and consequently it is also not possible to observe the present time dependence of diffusivities, which is dominant in this temperature region. In experiments with classical methods no modification of the starting profile is expected. The experimentally derived diffusivities shown in Fig. 4(a) are time-averaged diffusivities, D^{av}, which are given by

$$D^{av}(t) = \frac{1}{t}\int_{t_0}^{t} D(t')dt' \tag{2}$$

for $t_0=0$.[16] Here, D is the instantaneous diffusivity. In Fig. 4(c) the quantity

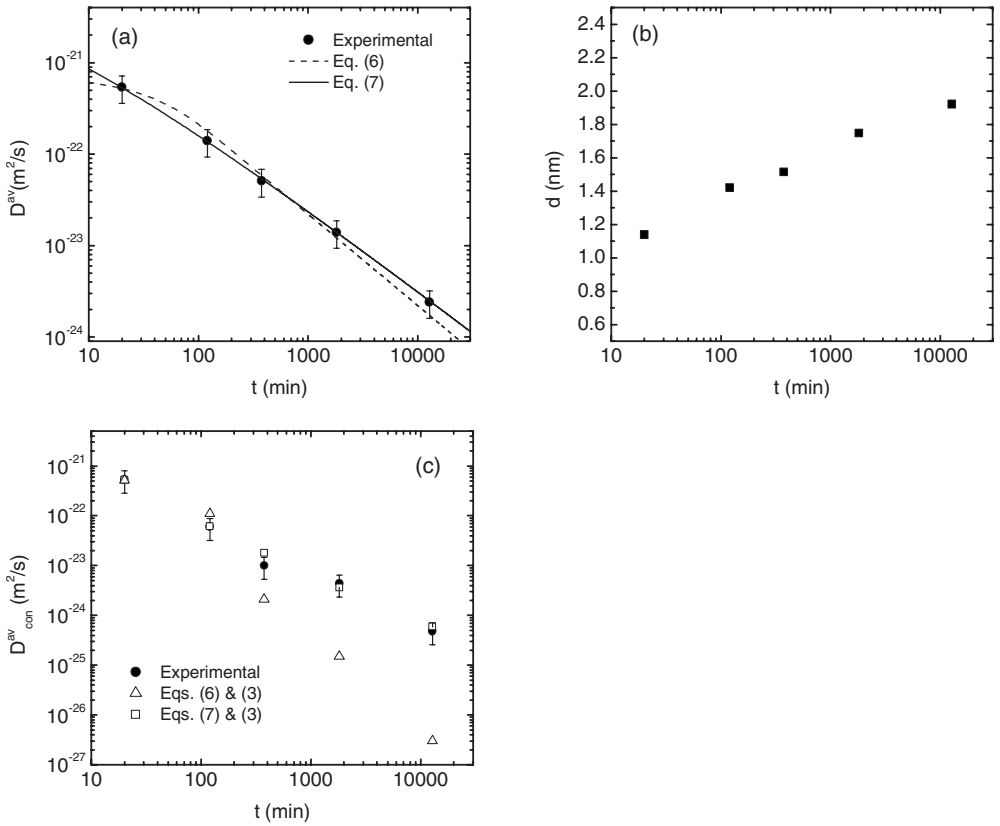

FIG. 4. Self-diffusivities in nanocrystalline Fe as a function of annealing time at 360 °C. Shown are (a) average diffusivities, D^{av}, (b) the corresponding diffusion lengths, and (c) consecutive average diffusivities, D^{av}_{con}. In (a) fits are also given as straight lines, using Eq. (7) and the parameters $D_0=4.1\times10^{-21}$ m^2/s, $D_E=3.0\times10^{-27}$ m^2/s, and $\tau=0.8$ min or alternatively Eq. (6) and $D_0=7.1\times10^{-22}$ m^2/s, $D_E=3.0\times10^{-27}$ m^2/s, and $\tau=31$ min.

$$D^{\mathrm{av}}_{\mathrm{con}}(t_{i+1}) = \frac{D^{\mathrm{av}}(t_{i+1})t_{i+1} - D^{\mathrm{av}}(t_i)t_i}{(t_{i+1} - t_i)} \tag{3}$$

is shown, which is calculated from the consecutive experimental diffusivities for annealing times of t_{i+1} and t_i. These values are a crude approximation for the instantaneous diffusivities present at time t_{i+1}. It can be seen that at 360 °C both quantities, D^{av} and $D^{\mathrm{av}}_{\mathrm{con}}$, decrease as a function of annealing time, while a constant value is not reached for the largest annealing time used in this study.

The time dependence of the diffusivities can be explained to be the result of defect annihilation processes. Self-diffusion in iron is generally governed by a vacancy-atom exchange process, where $D_{\mathrm{Fe}}=c_{\mathrm{D}}\ D_{\mathrm{D}}$ is valid. Here, D_{Fe} is the diffusivity of the Fe atoms, c_{D} is the atomic fraction of the defects governing diffusion, and D_{D} is the diffusivity of the defects. We assume now that at the beginning of the annealing process a large number of defects are present in excess to the thermal equilibrium value. These defects are formed due to knock-on effects during the sputter process and can be visualized as frozen-in nonequilibrium defects. Consequently, diffusion is governed by these excess point defects. During further annealing the number of point defects is reduced due to annihilation at sinks, a process which leads to a decrease in diffusivities. This annihilation process is most efficient at the beginning, however, also for very long annealing times up to several days an equilibrium state is not reached and defects are still annihilated.

Such defect-annihilation behavior is well known from diffusion studies in amorphous and glassy materials, such as silicate glasses,[17] metallic amorphous alloys,[18] and also covalent amorphous semiconductors.[19] There, it is generally described to be the result of structural relaxation processes, which lead to a rearrangement of short-range disorder during annealing and also to the annihilation of free volume or localized defects. Here, in case of volume diffusion in nanocrystalline materials, defect annihilation is the consequence of the nonequilibrium state in which nanomaterials are present after their synthesis. The observed strongly time-dependent volume diffusivities are an inherent property of this class of materials. A decrease in diffusivities in grain boundaries by defect annihilation was already observed to be the consequence of grain-boundary relaxation.[7] With the present measurements, the direct evidence was given, that defects in the grain interior also significantly modify diffusion in nanocrystalline metals due to annihilation processes.

The time dependence of D during relaxation is often described by a first-order reaction[16] as

$$D(t) = D_E + (D_0 - D_E)\exp\left(-\frac{t}{\tau}\right) \tag{4}$$

with D_0 as the initial diffusivity at $t=0$, D_E as the diffusivity in the equilibrium (relaxed) state, and τ as a typical time constant of relaxation or annihilation. Alternatively a second-order process (bimolecular annihilation) is often used in the free volume theory of glasses,[20] which can also be used to describe the time-dependent diffusivities according to

$$D(t) = D_E + (D_0 - D_E)\frac{1}{1 + t/\tau}. \tag{5}$$

Introducing Eq. (4) or alternatively Eq. (5) into Eq. (2) we obtain

$$D^{\mathrm{av}}(t) = D_E + (D_0 - D_E)\frac{\tau}{(t - t_0)}\left[\exp\left(-\frac{t_0}{\tau}\right) - \exp\left(-\frac{t}{\tau}\right)\right] \tag{6}$$

or

$$D^{\mathrm{av}}(t) = D_E + (D_0 - D_E)\frac{\tau}{(t - t_0)}\ln\left[\frac{1 + t/\tau}{(1 + t_0/\tau)}\right], \tag{7}$$

respectively. Least-squares fits of Eq. (6) and (7) to the experimental data for $t_0=0$ are shown in Fig. 4(a). As obvious, both types of equations describe the experimental data very well for parameters given in the caption of Fig. 4(a). The problem is that none of the three fitting parameters D_0, D_E, and τ can be determined unambiguously. For D_E we used the diffusivity which is obtained by an extrapolation of literature data on diffusion in Fe single crystals (for details see below).[21] D_0 and τ are strongly correlated quantities in the present case. For example, using $D_0=4.1\times10^{-21}$ m^2/s and $\tau=0.8$ min or $D_0=2.5\times10^{-20}$ m^2/s and $\tau=0.08$ min in Eq. (7) to describe the data gives essentially the same fitting curve. The same is true using Eq. (6). This result is due to the fact that the characteristic time constant of the annihilation process is below 20 min, the minimum annealing time used in this study. In order to obtain unambiguous fitting results it would be necessary to carry out additional measurements for annealing times below 20 min, e.g., by rapid thermal annealing. Generally, the characteristic time constant τ strongly depends on temperature, meaning that at lower temperatures this quantity increases. At 310 °C, the lowest temperature of our study, we can assess $\tau=(2.0\pm1.9)$ min and $D_0=(1.4\pm{}^{11.6}_{0.45})\times10^{-21}$ m^2/s, respectively. At temperatures of 360 °C and above only an upper limit of τ and a lower limit of D_0 can be obtained.

In order to decide which of the two annihilation models is valid here, we inserted functional values given by Eq. (6) and (7), respectively, into Eq. (3) for $t_0=t_i$ and $t=t_{i+1}$ and calculated the consecutive diffusivities for comparison to the experimental data in Fig. 4(c). As obvious, the diffusivities obtained from Eq. (7) describe the experimental data much better than those of Eq. (6). We conclude that the bimolecular model is better suited to describe defect annihilation in nanocrystalline Fe.

Also shown in Fig. 4(c) are the diffusivities $D^{\mathrm{av}}_{\mathrm{con}}(t_{\mathrm{max}})=D_{\mathrm{max}}$ obtained from the two highest annealing times according to Eq. (3), which are in good approximation to the instantaneous diffusivity at long annealing times, D_E. The diffusivities after 20 min of annealing, termed D_{20}, correspond to an averaging over the first annealing step (see Table I). Both quantities are plotted in Fig. 5 as a function of reciprocal temperature in comparison to literature data. It is obvious that the initial diffusivities, D_{20}, are significantly enhanced compared to data obtained at single crystals.[21] However, they are also significantly lower than literature data on

TABLE I. Diffusivity after 20 min of annealing, D_{20}, maximum annealing time and diffusivity at the maximum annealing time, D_{max}, for the temperatures under investigation.

Temperature (°C)	D_{20} (m^2/s)	t_{max} (h)	D_{max} (m^2/s)
310	2.4×10^{-22}	194	2.8×10^{-25}
360	5.5×10^{-22}	213	5.0×10^{-25}
380	5.5×10^{-22}	27	2.2×10^{-24}
400		231	2.3×10^{-24}
430	1.1×10^{-21}	221	1.8×10^{-24}
460	1.5×10^{-21}	146	7.0×10^{-24}
510	2.2×10^{-21}	1.5	3.0×10^{-22}

type-B and type-C grain-boundary diffusion in coarse-grained materials[22,23] and on nanocrystalline Fe showing considerable grain growth during the diffusion experiment[11] as well as on dislocation diffusion.[24] Least-squares fitting of these data to the Arrhenius equation is not meaningful here because the data correspond to different stages of the defect-annealing process at different temperatures. Nevertheless, the temperature dependence points to a relatively low activation enthalpy of diffusion smaller than 1 eV. Such a low activation enthalpy becomes understandable if we keep in mind that diffusion in the early stages is dominated by structural defects, meaning the activation enthalpy is the enthalpy of defect migration ($\Delta H=\Delta H_m$) and not given by a sum of a formation and a migration part, as observed in classical thermally equilibrated metallic systems ($\Delta H=\Delta H_f+\Delta H_m$). Recent theoretical *ab initio* calculations in the framework of density-functional theory within the generalized gradient approximation with spin polarization using the SIESTA code give migration enthalpies in bcc iron of 0.34 eV for single interstitials, as well as of 0.67 eV for single vacancies.[25] By a comparison to our experimental findings we conclude that atomic migration in the initial state very likely takes place with highly mobile Fe interstitials or vacancies.

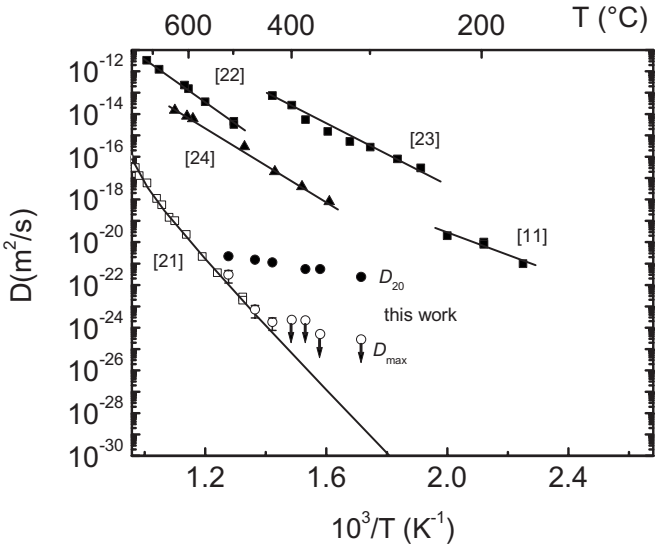

FIG. 5. Self-diffusivities in nanocrystalline Fe as a function of reciprocal temperature in comparison to literature data. Shown are D_{20} and D_{max} of this work as well as literature data on volume diffusion in single crystals (Ref. 21), type B grain-boundary diffusion in coarse-grained Fe (Ref. 22), type C grain-boundary diffusion in coarse-grained Fe (Ref. 23), type C grain-boundary diffusion in nanocrystalline Fe with an unstable nanostructure (Ref. 11), and dislocation diffusion in coarse-grained Fe (Ref. 24). The arrows indicate upper limits.

The diffusivities determined for the maximum annealing times, D_{max} (see Table I and Fig. 5), can be subdivided into two groups. For temperatures above 400 °C a final equilibrium state is reached, where the instantaneous diffusivities are no longer time dependent. As obvious from Fig. 5 these diffusivities are in good accordance with volume diffusivities obtained by the radiotracer method.[21] This demonstrates that at these temperatures, defect annihilation is nearly complete and diffusion takes place via thermal vacancies. However, at temperatures below 400 °C defect annihilation is a still ongoing process. Diffusivities as low as 5×10^{-25} m^2/s still decrease significantly during annealing. For the maximum annealing times used in this study of more than 8 days, an equilibrium state is not reached. The important finding from our neutron reflectometry measurements is that in sputtered nanocrystalline Fe samples at temperatures below 400 °C diffusion cannot easily be described by an extrapolation of high-temperature volume diffusivities to lower temperatures. Defect-annihilation processes dominate the long-time diffusion behavior at low temperatures.

It has to be stated that experiments using neutron reflectometry on as-sputtered isotope multilayer films for short annealing times always should give diffusivities higher than values obtained for annealed single crystals by classical tracer diffusion techniques. It is an unavoidable limitation of the method if it is applied on as-sputtered samples for the determination of very low diffusivities. Careful long-term anneals up to several days have to be carried out until an equilibrium state is reached and values of single crystals can be reproduced. This is especially important for the exploration of new unknown systems. Note that if isotope multilayers are produced in form of single crystals by molecular-beam epitaxy the upper limitation is not valid, as recently demonstrated by self-diffusion measurements in Germanium.[13] Here, no time-dependent diffusivities are observed at low temperatures since this deposition method produces a significant lower concentration of nonequilibrium defects.

The present findings on Fe have also important consequences for the possibility to detect grain-boundary diffusion in nanocrystalline metals by neutron reflectometry and isotope multilayers. This is possible only in regime of type C kinetics regime of Harrison's classification,[15] where volume diffusion is frozen-in and atomic transport exclusively takes place along grain boundaries. This regime is generally defined to be present at $(D_V t)^{0.5} < \delta/20$, where $\delta \approx 0.5$ nm is the grain-boundary diameter and D_V is the volume diffusivity, meaning that the (hypothetical) volume diffusion length has to be below 0.035 nm. If an extrapolation of the volume diffusivities obtained by the radiotracer technique[21] is assumed (see Fig. 5), this criterion is fulfilled for temperatures below 440 °C for reasonable annealing times larger than 10

min. However, taking the initial volume diffusivities, D_{20}, found in this study on the order of 10^{-21} m^2/s, at 310 °C type C diffusion cannot be reached for reasonable annealing times. However, type C grain boundary might be observed for temperatures below 200 °C. At these temperatures defect annihilation in volume is also expected to be so slow that a temporal separation of the contributions of volume diffusion and grain-boundary diffusion to the Bragg-peak decrease should be possible. Such experiments are in progress.

In order to attribute the question whether an oxidation of Fe due to water vapor or oxygen might influence diffusion, the following points have to be addressed; (a) oxide inclusions cannot be found inside the film by TEM and selected area electron-diffraction measurements. (b) From analysis with grazing incidence x-ray diffraction we find no indication for an oxide phase for $T<400$ °C. (c) In the as-deposited state there already exists a small oxide top layer with a thickness of only 2 nm as supported by x-ray reflectivity (XRR) measurements. Such layers are always formed after the transfer of the sputtered film into air. XRR measurements show that this oxide film does not grow during annealing at 400 °C. (d) At temperatures above 400 °C we obtain the same diffusivities $D_{\max}$ as for single crystals, indicating a negligible influence of oxidation on diffusion. (e) The effect which determines our diffusivity (decay of the Bragg peak) results from a modification of the scattering length density inside the film and not at the surface. Consequently, an influence of an oxide layer on diffusion cannot be completely ruled out but due to the upper argumentation we believe that there is no significant effect.

IV. CONCLUSIONS

We demonstrated by neutron reflectometry experiments on $[^{57}\mathrm{Fe}(7\ \mathrm{nm})/^{\mathrm{nat}}\mathrm{Fe}(3\ \mathrm{nm})]_{15}$ isotope multilayers that it is possible to detect volume self-diffusivities in Fe at low temperatures in a nanostructure, which is not being significantly modified by grain growth during annealing. The method used was able to detect point-defect annihilation processes, which lead to time-dependent diffusivities during isothermal annealing. The diffusion lengths during this process are between 0.8 and 2.5 nm, not detectable with classical methods of diffusivity determination. For very long annealing times the diffusivities above 400 °C are in good accordance with the volume diffusivities given in literature. However, at temperatures below 400 °C the diffusivities are higher than the literature data, indicating that defect annihilation is still going on for up to 8 days of annealing. As a result, nanocrystalline Fe produced by ion-beam sputtering has, in comparison to thermodynamically stable single crystalline or polycrystalline samples, an increased concentration of structural defects, which dominate the atomic transport.

ACKNOWLEDGMENTS

Support by the German Research Foundation (DFG) is gratefully acknowledged. This work is based on experiments performed at the Geesthacht Neutron Facility (GENF).

*harald.schmidt@tu-clausthal.de

[1] I. A. Ovid'ko, Science **295**, 2386 (2002).
[2] K. S. Kumar, H. Van Swygenhoven, and S. Suresh, Acta Mater. **51**, 5743 (2003).
[3] H. Van Swygenhoven and J. R. Weertman, Mater. Today **9**, 24 (2006).
[4] K. S. Siow, A. A. O. Tay, and P. Oruganti, Mater. Sci. Technol. **20**, 285 (2004).
[5] J. Weissmüller and J. Markmann, Adv. Eng. Mater. **7**, 202 (2005).
[6] H. Natter, M. Schmelzer, M. S. Löffler, C. E. Krill, A. Fitch, and R. Hempelmann, J. Phys. Chem. B **104**, 2467 (2000).
[7] R. Würschum, S. Herth, and U. Brossmann, Adv. Eng. Mater. **5**, 365 (2003).
[8] C. E. Krill III, L. Helfen, D. Michels, H. Natter, A. Fitch, O. Masson, and R. Birringer, Phys. Rev. Lett. **86**, 842 (2001).
[9] Y. Estrin, G. Gottstein, E. Rabkin, and L. S. Shvindlman, Acta Mater. **49**, 673 (2001).
[10] W. Brückner and V. Weihnacht, J. Appl. Phys. **85**, 3602 (1999).
[11] H. Tanimoto, P. Farber, R. Würschum, R. Z. Valiev, and H.-E. Schäfer, Nanostruct. Mater. **12**, 681 (1999).
[12] H. Schmidt, M. Gupta, and M. Bruns, Phys. Rev. Lett. **96**, 055901 (2006).
[13] E. Hüger, U. Tietze, D. Lott, H. Bracht, D. Bougeard, E. E. Haller, and H. Schmidt, Appl. Phys. Lett. **93**, 162104 (2008).
[14] H. Schmidt, M. Gupta, J. Stahn, T. Gutberlet, and M. Bruns, Acta Mater. **56**, 464 (2008).
[15] L. G. Harrison, Trans. Faraday Soc. **57**, 1191 (1961).
[16] F. Faupel, W. Frank, M. P. Macht, H. Mehrer, V. Naundorf, K. Rätzke, H. R. Schober, S. K. Sharma, and H. Teichler, Rev. Mod. Phys. **75**, 237 (2003).
[17] U. Buchenau, H. M. Zhou, N. Nucker, K. S. Gilroy, and W. A. Phillips, Phys. Rev. Lett. **60**, 1318 (1988).
[18] A. Van Den Beukel and S. Radelaar, Acta Metall. **31**, 419 (1983).
[19] H. Schmidt, W. Gruber, T. Gutberlet, M. Ay, J. Stahn, U. Geckle, and M. Bruns, J. Appl. Phys. **102**, 043516 (2007).
[20] F. Spaepen, Acta Metall. **25**, 407 (1977).
[21] M. Lübbehusen and H. Mehrer, Acta Metall. Mater. **38**, 283 (1990).
[22] S. V. Divinski, J. Geise, E. Rabkin, and C. Herzig, Z. Metallkd. **95**, 945 (2004).
[23] A. Inoue, H. Nitta, and Y. Iijima, Acta Mater. **55**, 5910 (2007).
[24] Y. Iijima, J. Phase Equilib. Diffus. **26**, 466 (2005).
[25] C. C. Fu, J. Dalla Torre, F. Willaime, J. L. Bocquet, and A. Barbu, Nature Mater. **4**, 68 (2005).